Prediction of Interpolants in Subsampled Radargram Slices

T. Kishan Rao[1], E. G. Rajan[2], Dr. M Shankar Lingam[3]

[1]Research Scholar, MG-NIRSA, University of Mysore, Mysuru, Karnataka, India

[1]Former Executive Engineer, Irrigation Department, Government of Telangana, Telangana, India

[2]Adjunct Professor, Department of Cybernetics,
University of Petroleum and Energy Studies, Dehradun, Uttarakhand, India

[2]Hon. Director MG-NIRSA, Hyderabad, India

[3]Research Associate, NIRDPR, Hyderabad, India

ABSTRACT
This paper provides an algorithmic procedure to predict interpolants of subsampled images. Given a digital image, one can subsample it by forcing pixel values in the alternate columns and rows to zero. Thus, the size of the subsampled image is reduced to half of the size of the original image. This means 75% of the information in the original image is lost in the subsampled image. The question that arises here is whether it is possible to predict these lost pixel values, which are called interpolants so that the reconstructed image is in accordance with the original image. In this paper, two novel interpolant prediction techniques, which are reliable and computationally efficient, are discussed. They are (i) interpolant prediction using neighborhood pixel value averaging and (ii) interpolant prediction using extended morphological filtering.

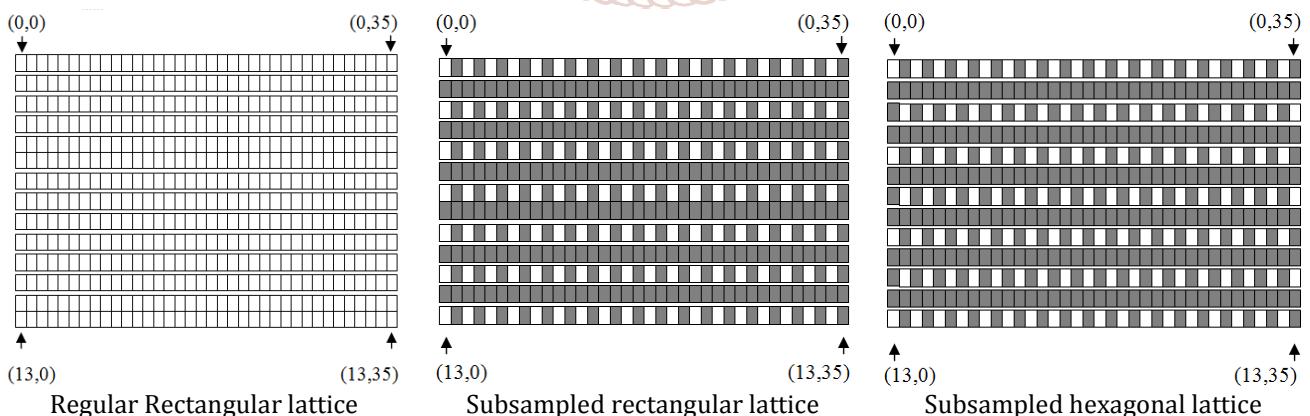*KEYWORDS: Ground Penetrating Radar, Subsurface Imaging, Targeted Buried Object Detection, Interpolant Prediction*

1. INTRODUCTION
Concept of Subsampling
Fig. 1 shows the result of rectangular and hexagonal subsampling of an array of size 36x14. In both cases, pixel values of alternate rows are made '0' and alternate pixel values of each row are made '0' as shown in Fig. 1.

Fig. 1: Rectangular and hexagonal subsampling of digital images

(0,0) ... (0,35)   (13,0) ... (13,35)
Regular Rectangular lattice   Subsampled rectangular lattice   Subsampled hexagonal lattice

Algorithm for rectangular sub sampling

pixel_val_rect_subsampled(i, j)   = pixel_val(2i, 2j); if i is even
                                    = pixel_val(2i, 2j); if i is odd

Algorithm for hexagonal sub sampling

pixel_val_hex_subsampled(i, j)   = pixel_val(2i, 2j); if i is even
                                    = pixel_val(2i, 2j + 1); if i is odd

Only rectangular subsampling is considered here. Fig. 2 shows a sample image of size 1177×891 and its rectangular subsampled version. Fig. 3 shows a sample radargram image slice of size 256×256 and its rectangular subsampled version.

Sample gold mine image   Its rectangular subsampled version
Fig. 2: Sample gold mine image and its rectangular subsampled version
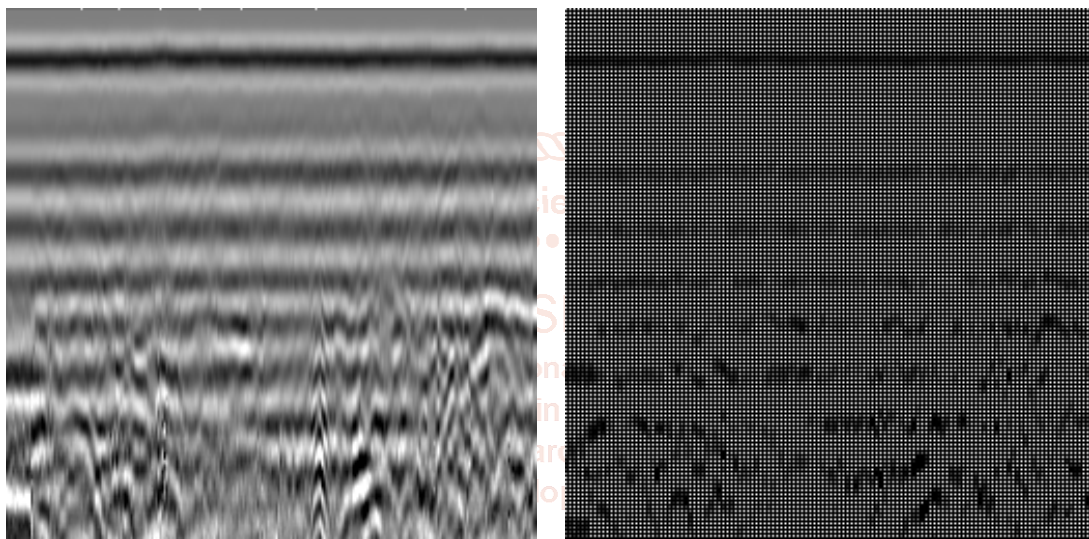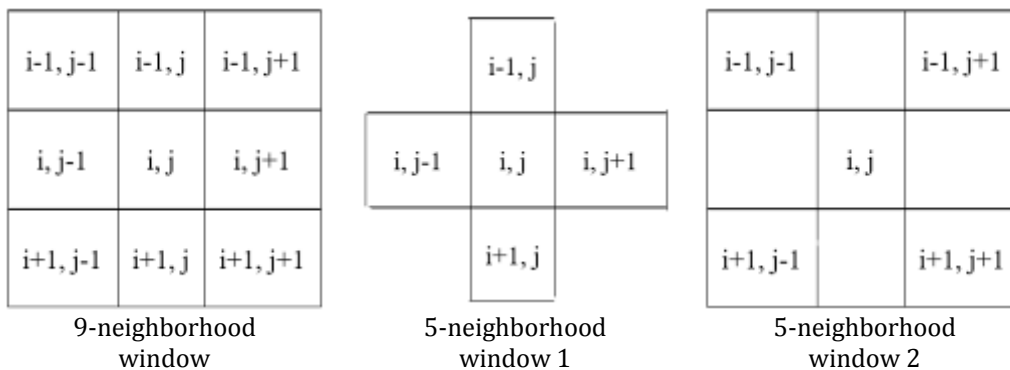

Sample radargram image slice   Its rectangular subsampled version
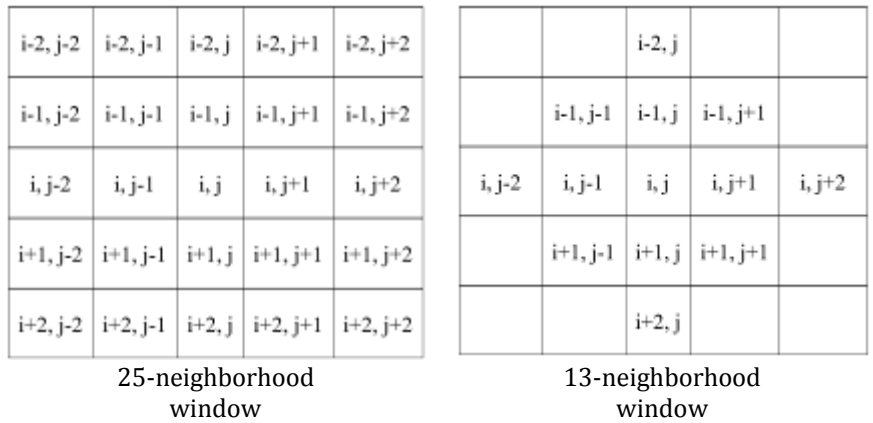**Fig. 3: Sample radargram image slice and its rectangular subsampled version**

The rectangular subsampled versions of the gold mine image and the radargram image slice are respectively shown in Fig. 2 and Fig. 3. The question that arises here is whether it is possible to estimate or predict the unknown interpolant pixel values in subsampled images, denoted by '0s'. One can make use of spatial and spectral domain transforms based prediction techniques for evaluating the unknown interpolant pixel values in a subsampled image. Two novel interpolant prediction techniques, which are reliable and computationally efficient, are discussed in this paper. They are (i) interpolant prediction using neighborhood pixel value averaging and (ii) interpolant prediction using extended morphological filtering. Basic details of these two techniques are briefly outlined in the following.

2. Interpolant Prediction Techniques
2.1. Interpolant prediction using neighborhood pixel value averaging
This is a computationally intensive process for interpolant prediction.

9-neighborhood   5-neighborhood   5-neighborhood
window   window 1   window 2

i-2, j-2	i-2, j-1	i-2, j	i-2, j+1	i-2, j+2
i-1, j-2	i-1, j-1	i-1, j	i-1, j+1	i-1, j+2
i, j-2	i, j-1	i, j	i, j+1	i, j+2
i+1, j-2	i+1, j-1	i+1, j	i+1, j+1	i+1, j+2
i+2, j-2	i+2, j-1	i+2, j	i+2, j+1	i+2, j+2

25-neighborhood window

		i-2, j		
	i-1, j-1	i-1, j	i-1, j+1	
i, j-2	i, j-1	i, j	i, j+1	i, j+2
	i+1, j-1	i+1, j	i+1, j+1	
		i+2, j		

13-neighborhood window

Fig. 4: Basic scanning windows used in image processing

Scan the subsampled image with the 9-neighborhood window shown in Fig. 4. At every position, the interpolant is evaluated as the average of all available non-zero values using the prediction formula

$$\frac{\{x(i-1, j-1)+x(i-1, j)+x(i-1, j+1)+x(i, j-1)+x(i, j+1)+ x(i+1, j-1)+ x(i+1, j)+ x(i+1, j+1)\}}{n}$$

where n is the number of non-zero pixel values. The algorithm is applied to the whole image.

Fig. 5 shows subsampled image of the gold mine image and the reconstructed image using the interpolant prediction formula. Fig. 6 shows subsampled image of the radargram image slice and the reconstructed image using the interpolant prediction formula.

Gold mine image subsampled   Reconstructed version of subsampled image

Fig. 5: Reconstructed image from subsampled version of gold mine image using prediction formula
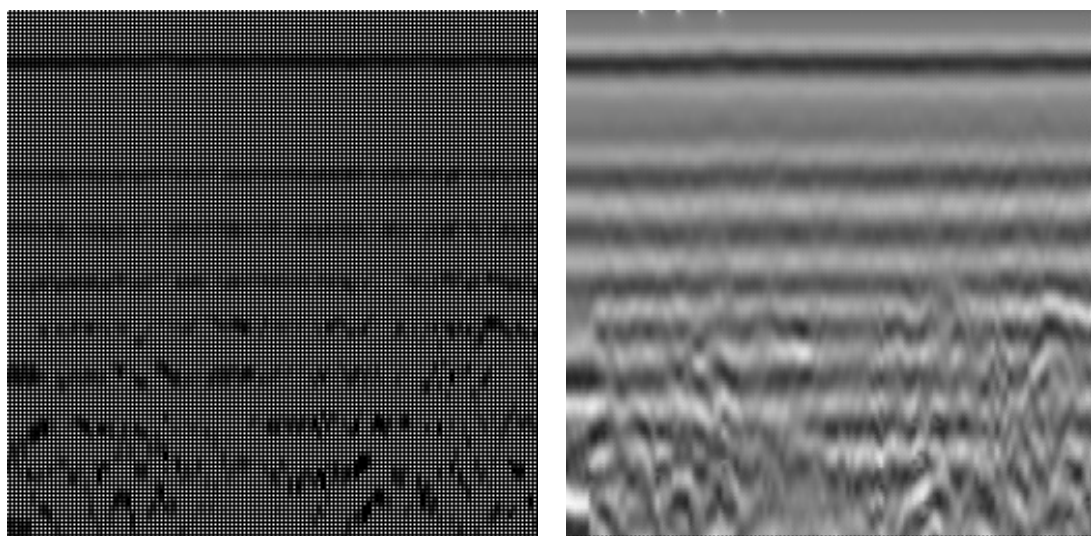
Radargram image slice subsampled   Reconstructed version of subsampled image

Fig. 6: Reconstructed image from subsampled version of radargram image using prediction formula

2.2. Interpolant prediction using extended morphological filtering

Morphological filtering makes use of two fundamental operations of 'dilation' and 'erosion', which are defined as follows.

Dilation: Let image to be dilated be A and the structuring element that dilates A be B. Then the dilation of A by B is defined as the Minkowski addition $D(A,B) = A \oplus B = \text{EXTSUP}_{(x,y) \in D_B}[A_{x,y} + B(x,y)]$, where D_B is the domain of the image B, and EXTSUP is an operation of supremum over the union of the domains.

Erosion: Let image to be eroded be A and the structuring element that erodes A be B. Then the erosion of A by B is defined as the Minkowski subtraction $A\theta B = \text{INF}_{(x,y) \in D_B}[A_{x,y} + B(x,y)]$ as $E(A,B) = \text{INF}_{(x,y) \in D_B}[A_{-x,-y} - B(x,y)]$, where D_B is the domain of the image B, and INF is an operation of infimum over the intersection of the domains.

Following these definitions, morphological filtering operations of **Closing** and **Opening** are defined in the following manner. Closing of A by B is represented as AoB and defined as AoB = $(A \oplus B)\theta B$. Opening of A by B is represented as A•B and defined as A•B = $(A\theta B) \oplus B$. Same structuring element should be used for dilation and erosion in any morphological filtering. Closing and opening are idempotent operators. (AoB)o(AoB) = AoB and (A•B)•(A•B) = A•B

2.2.1. Extended morphological filters
These are essentially morphological filters except that the structuring element need not remain the same for dilation and erosion in any morphological filtering. With reference to Fig. 7, for example, one can use the structuring element E11337799 for dilation and subsequently E1379 for erosion, so that extended closing operation is carried out on a given image. The structuring elements of E11337799 and E1379 are shown in the respective dialog boxes. Extended morphological filtering is a computationally less intensive process for interpolant prediction. At every position, the interpolant is evaluated using the procedure given below. Scan the given subsampled image and dilate it with E-11337799 shown in Fig. 7. Subsequently, erode with E-1379 shown in Fig. 7. The resulting image is extended morphological filtered version, which is also the interpolant predicted version.

Information loss due to rectangular subsampling
Given an image of size 100×100, size of its subsampled version turns out to be 50×50. The number of pixels in the subsampled version is 2,500, whereas number of pixels in the original image is 10,000. This means 75% of information contained in the original image is lost by subsampling it.

Neighborhood structure E-11337799   Neighborhood structure E-1379
Fig. 7: Structuring elements used for extended morphological filtering

Image reconstruction
By extended morphological filtering, one can reconstruct the original image from the subsampled version, which means the lost information is predicted. Let us take some sample images and do the process of subsampling and extended morphological filtering. Fig. 8 shows a sample image of a gold mine, its subsampled version, the subsampled image dilated using structuring element E-11337799 and the dilated image eroded again using structuring element E-1379. Scan subsampled image with E-11337799. At every position, find the maximum image pixel value and assign it to the central pixel and thus dilation is carried out. Then, scan dilated version of subsampled image with E-1379. At every position, find the minimum image pixel value and assign it to the central pixel and thus erosion is carried out. By virtue of this reconstruction process, 75% of the lost information due to subsampling is recovered with maximum accuracy.

Sample gold mine image   Its rectangular subsampled version

Subsampled image dilated
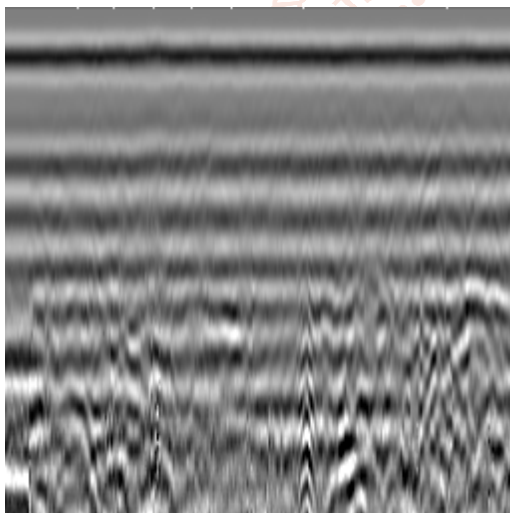with E11337799 Structuring element

Subsampled and dilated image eroded
with E1379 structuring element

**Fig. 8: Sample gold mine image subsampled and then reconstructed morphologically**

On the same lines, Fig. 9 shows a sample image of a radargram image slice, its subsampled version, the subsampled image dilated using structuring element E-11337799 and the dilated image eroded again using structuring element E-1379. Scan subsampled image with E-11337799. At every position, find the maximum image pixel value and assign it to the central pixel and thus dilation is carried out. Then, scan dilated version of subsampled image with E-1379. At every position, find the minimum image pixel value and assign it to the central pixel and thus erosion is carried out.

Comparative study of prediction using neighborhood pixel value averaging and extended morphological filtering
A comparative study is made on the two interpolant prediction techniques in terms of statistical analysis. Statistical parameters include mean, median and standard deviation based on saturation, luminance, Cb, Cr and White Balance (WB). Visual quality is also another measure by which one can compare the two techniques. However, due to space restriction, this paper provides results of comparative study based on statistical parameters only.

Sample radargram image slice
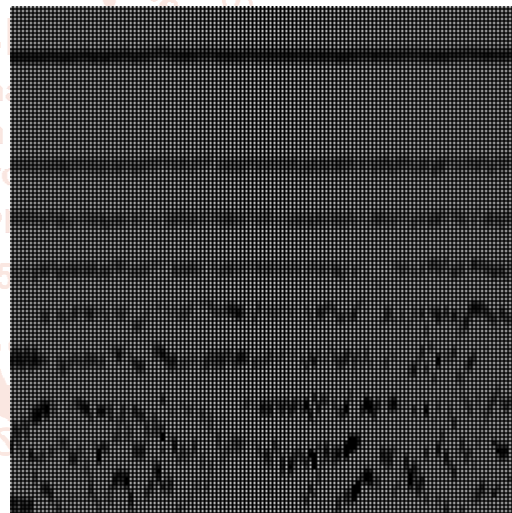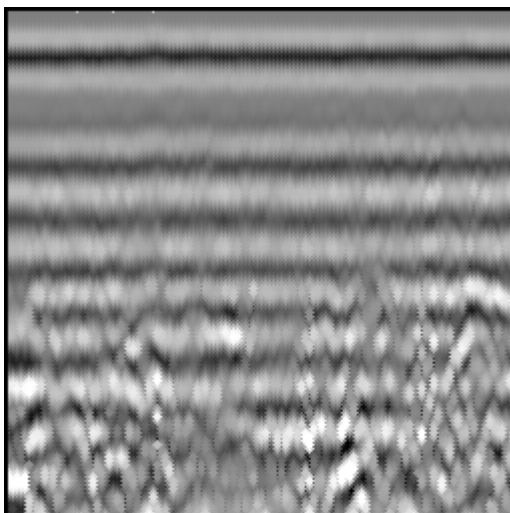
Its rectangular subsampled version

Subsampled image dilated
with E11337799 Structuring element

Subsampled and dilated image eroded
with E1379 structuring element

Fig. 9: Sample radargram image slice subsampled and then reconstructed morphologically

2.3. **Statistical parameters of gold mine image, its subsampled image, and reconstructed images using prediction formula and extended morphological filter**

The statistical parametric values of the original gold mine image, its subsampled and the reconstructed images using prediction formula and extended morphological filter are presented in Table 1.

Table 1: Statistics of the original gold mine image, its subsampled image and the reconstructed images using prediction formula and extended morphological filter
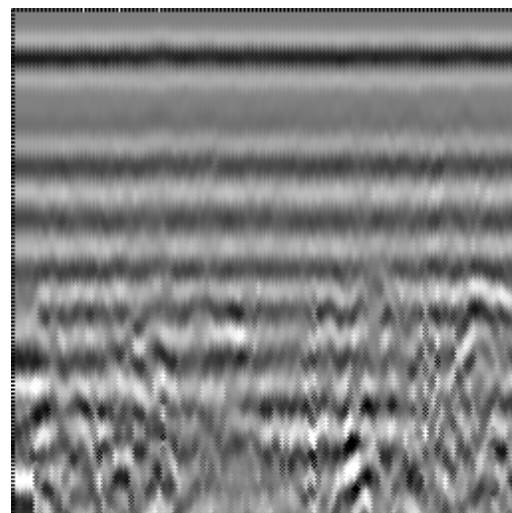
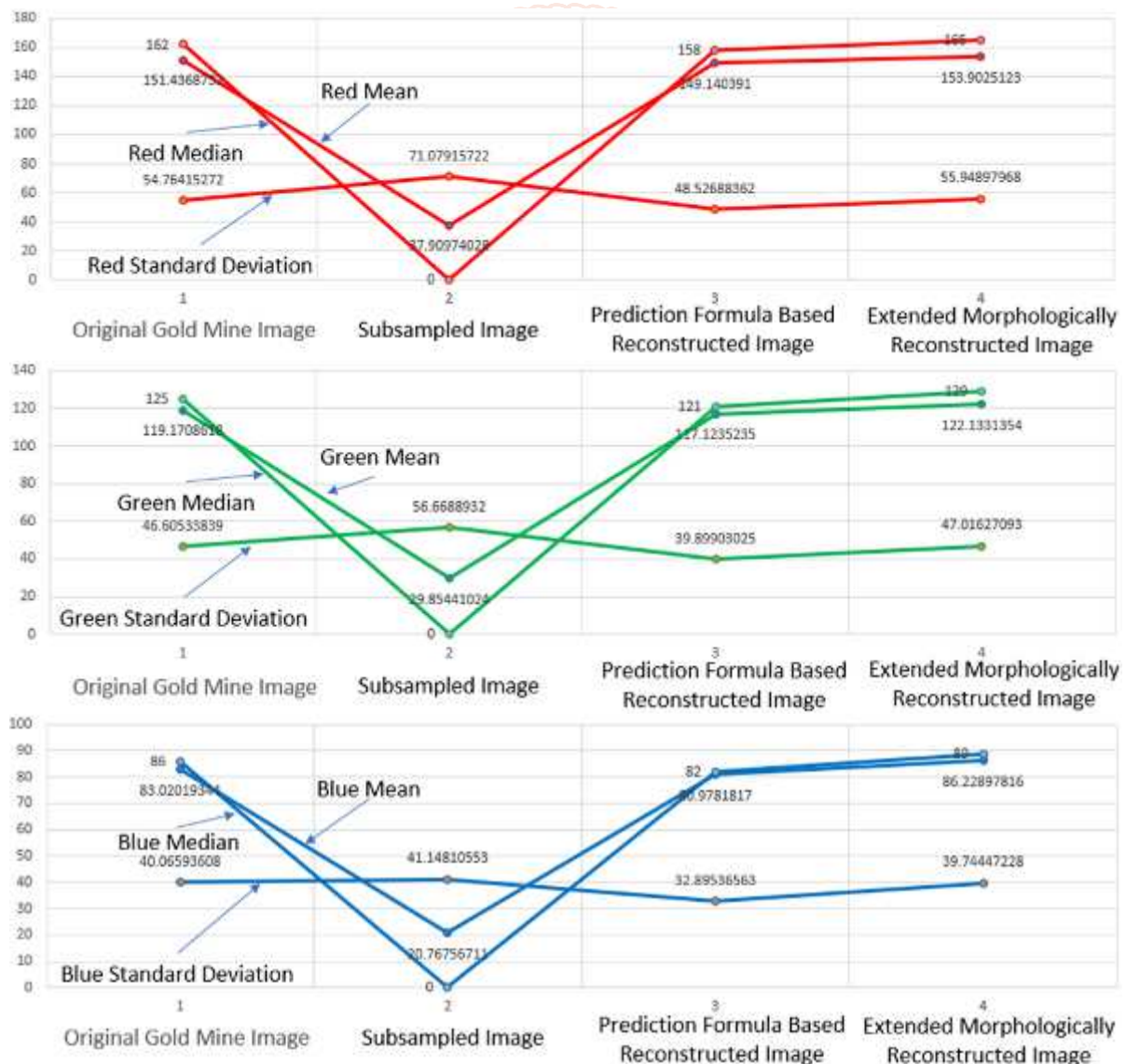| Statistical Parameters	Parametric Values of Original Gold Mine Image	Parametric Values of Subsampled Image	Parametric Values of Prediction Formula Based Reconstructed Image	Parametric Values of Morphologically Reconstructed Image
Pixels Count	1048707	1048707	1048707	1048707
Pixels without black	1048576	262657	1048706	1035102
Red Min	0	0	0	0
Red Max	255	255	255	255
Red Mean	151.436873216256	37.9097402801736	149.140390976698	**153.902512331852**
Red Standard Deviation	54.7641527176397	71.0791572237396	48.5268836177345	**55.9489796839469**
Red Median	162	0	158	**165**
Red Total Count	1048707	1048707	1048707	1048707
Green Min	0	0	0	0
Green Max	244	244	225	244
Green Mean	119.170861832714	29.8544102404199	**117.123523538987**	122.133135375276
Green Standard Deviation	46.6053383895709	56.66889319849	39.8990302499627	**47.0162709280861**
Green Median	125	0	**121**	**129**
Green Total Count	1048707	1048707	1048707	1048707
Blue Min	0	0	0	0
Blue Max	213	213	208	213
Blue Mean	83.0201934382053	20.7675671088302	**80.9781817037552**	**86.2289781607255**
Blue Standard Deviation	40.0659360770024	41.1481055277849	32.8953656258832	**39.7444722827248**
Blue Median	86	0	82	**89**
Blue Total Count	1048707	1048707	1048707	1048707
Saturation Min	0	0	0	0
Saturation Max	1	1	1	1
Saturation Mean	0.414704293012619	0.103985674679279	0.370900481939316	0.396443426609039
Saturation Standard Deviation	0.162035375833511	0.197366669774055	0.0971372798085213	0.153284594416618
Saturation Median	0.384313732385635	0	0.360784322023392	0.376470595598221
Luminance Min	0	0	0	0
Luminance Max	0.917647063732147	0.917647063732147	0.874509811401367	0.917647063732147
Luminance Mean	0.458759993314743	0.114812918007374	0.450238972902298	0.469898104667664
Luminance Standard Deviation	0.183519154787064	0.218835264444351	0.157679125666618	0.185223534703255
Luminance Median	0.482352942228317	0	0.466666668653488	0.498039215803146
Y Min	0	0	0	0
Y Max	0.952941179275513	0.952941179275513	0.886274516582489	0.952941179275513
Y Mean	0.486793965101242	0.121905006468296	0.478467851877213	0.497977554798126
Y Standard Deviation	0.188331753015518	0.23099610209465	0.162625074386597	0.190497159957886
Y Median	0.513725519180298	0	0.498039215803146	0.529411792755127
Cb Min	-0.174509793519974	-0.174509793519974	-0.154901951551437	-0.174509793519974
Cb Max	0.0058823823928833	0.0058823823928833	-0.00196078419685364	0.0058823823928833
Cb Mean	-0.0942264795303345	-0.0251161027699709	-0.0940429195761681	-0.0934102386236191
Cb Standard Deviation	0.0280981101095676	0.0424498282372952	0.0265024919062853	0.0293857846409082
Cb Median	-0.0999999940395355	-0.00196078419685364	-0.0999999940395355	-0.0999999940395355
Cr Min	-0.0529411733150482	-0.0529411733150482	-0.02156862616539	-0.0529411733150482

Cr Max	0.158823549747467	0.15490198135376	0.147058844566345	0.15490198135376
Cr Mean	0.072875089943409	0.0167419668287039	0.0724304616451263	0.0718267410993576
Cr Standard Deviation	0.0252073612064123	0.0347290895879269	0.0238945260643959	0.0263226460665464
Cr Median	0.0803921818733215	-0.00196078419685364	0.0764706134796143	0.0803921818733215
Red Min WB	0	0	1	0
Red Max WB	255	255	255	255
Red Mean WB	151.455792427063	151.361699859513	149.140533190427	155.925350351946
Red Standard Deviation WB	54.741407379937	54.7700117815729	48.5266882169737	53.4417436019203
Red Median WB	162	162	158	166
Red Total Count WB	1048576	262657	1048706	1035102
Green Min WB	0	0	0	0
Green Max WB	244	244	225	244
Green Mean WB	119.185750007629	119.199294136459	117.123635222837	123.738408388739
Green Standard Deviation WB	46.5892097611166	46.6060051292808	39.8988853486659	45.1768767632341
Green Median WB	125	125	121	130
Green Total Count WB	1048576	262657	1048706	1035102
Blue Min WB	0	0	0	0
Blue Max WB	213	213	208	213
Blue Mean WB	83.0305652618408	82.9183802449583	80.9782589209941	87.3623401365276
Blue Standard Deviation WB	40.057690959735	40.0853869885363	32.8952862670455	38.7475406623176
Blue Median WB	86	86	82	90
Blue Total Count WB	1048576	262657	1048706	1035102
Saturation Min WB	0	0	0.0549019612371922	0
Saturation Max WB	1	1	1	1
Saturation Mean WB	0.414756119251251	0.415182173252106	0.370900839567184	0.401654124259949
Saturation Standard Deviation WB	0.161979168653488	0.162253737449646	0.0971366539597511	0.14735022187233
Saturation Median WB	0.384313732385635	0.384313732385635	0.360784322023392	0.376470595598221
Luminance Min WB	0.00392156885936856	0.00392156885936856	0	0.00392156885936856
Luminance Max WB	0.917647063732147	0.917647063732147	0.874509811401367	0.917647063732147
Luminance Mean WB	0.458817303180695	0.4584119617939	0.450239419937134	0.476074278354645
Luminance Standard Deviation WB	0.183458968997002	0.183562874794006	0.157678574323654	0.178377047181129
Luminance Median WB	0.482352942228317	0.482352942228317	0.466666668653488	0.501960813999176
Y Min WB	0	0	0	0
Y Max WB	0.952941179275513	0.952941179275513	0.886274516582489	0.952941179275513
Y Mean WB	0.486854791641235	0.486728459596634	0.478468328714371	0.504522800445557
Y Standard Deviation WB	0.188264891505241	0.188352286815643	0.162624478340149	0.182931467890739
Y Median WB	0.513725519180298	0.513725519180298	0.498039215803146	0.533333361148834
Cb Min WB	-0.174509793519974	-0.174509793519974	-0.154901951551437	-0.174509793519974
Cb Max WB	0.0058823823928833	0.0058823823928833	-0.00196078419685364	0.0058823823928833
Cb Mean WB	-0.0942380055785179	-0.0944127067923546	-0.0940430089831352	-0.094612218439579
Cb Standard Deviation WB	0.0280809327960014	0.0280743390321732	0.0265023522078991	0.0276316702365875
Cb Median WB	-0.099999940395355	-0.099999940395355	-0.099999940395355	-0.099999940395355
Cr Min WB	-0.0529411733150482	-0.0529411733150482	-0.02156862616539	-0.0529411733150482
Cr Max WB	0.158823549747467	0.15490198135376	0.147058844566345	0.15490198135376
Cr Mean WB	0.0728844404220581	0.0727134346961975	0.0724305287003517	0.0727965757250786
Cr Standard Deviation WB	0.0251950528472662	0.0252188909798861	0.023894427344203	0.0250895656645298
Cr Median WB	0.0803921818733215	0.0803921818733215	0.0764706134796143	0.0803921818733215

Observations
1. Median values become '0' for subsampled image. This phenomenon has been seen for all kinds of images.
2. The reconstructed image using prediction formula is pretty much closer to the original image.
3. The reconstructed image using extended morphological filter is pretty much closer to the original image.
4. There is an increase in the contrast in the reconstructed image when compared to the original image.

Fig. 10 shows a graphical presentation of the values of mean, standard deviation and median for red, green and blue components of the original gold mine image, its subsampled image and the prediction formula and morphological filter based reconstructed images.

Red Mean	151.436873216256	37.9097402801736	149.140390976698	**153.902512331852**
Red Standard Deviation	54.7641527176397	71.0791572237396	48.5268836177345	**55.9489796839469**
Red Median	162	0	158	**165**
Green Mean	119.170861832714	29.8544102404199	**117.123523538987**	122.133135375276
Green Standard Deviation	46.6053383895709	56.66889319849	39.8990302499627	**47.0162709280861**
Green Median	125	0	**121**	**129**
Blue Mean	83.0201934382053	20.7675671088302	**80.9781817037552**	**86.2289781607255**
Blue Standard Deviation	40.0659360770024	41.1481055277849	32.8953656258832	**39.7444722827248**
Blue Median	86	0	82	**89**

Fig. 10: Graphical presentation of the values of mean, standard deviation and median for red, green and blue components of the gold mine image, its subsampled image and the prediction formula and morphological filter based reconstructed images

2.4. Statistical parameters of radargram image slice, its subsampled image, and reconstructed images using prediction formula and extended morphological filter

The statistical parametric values of the original radargram image slice, its subsampled image and the reconstructed images using prediction formula and extended morphological filter are presented in Table 2.

Table 2: Statistics of the original radargram image slice image, its subsampled image and the reconstructed images using prediction formula and extended morphological filter

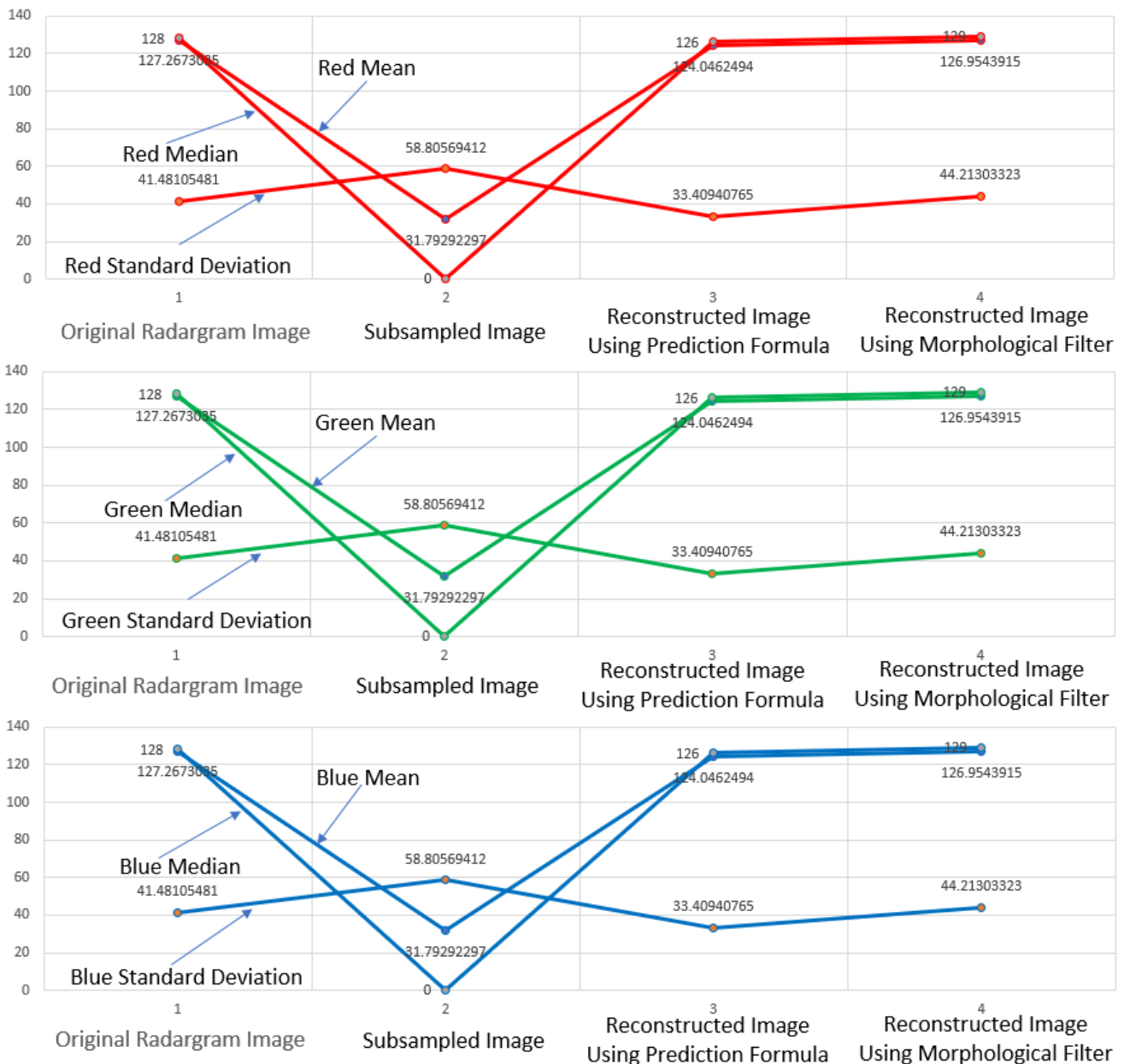| Statistical Parameters	Parametric values of Original Radargram Image	Parametric Values of Subsampled Image	Parametric Values of Prediction Formula Based Reconstructed Image	Parametric Values of Morphologically Reconstructed Image
Pixels Count	**65536**	65536	65536	65536
Pixels without black	65401	16353	65049	63944
Red Min	0	0	0	0
Red Max	255	255	255	255
Red Mean	127.267303466797	31.7929229736328	124.046249389648	**126.954391479492**
Red Standard Deviation	41.4810548080386	58.8056941224182	33.4094076505899	**44.2130332332022**
Red Median	128	0	126	**129**
Red Total Count	65536	65536	65536	65536
Green Min	0	0	0	0
Green Max	255	255	255	255
Green Mean	127.267303466797	31.7929229736328	124.046249389648	**126.954391479492**
Green Standard Deviation	41.4810548080386	58.8056941224182	33.4094076505899	**44.2130332332022**
Green Median	128	0	126	**129**
Green Total Count	65536	65536	65536	65536
Blue Min	0	0	0	0
Blue Max	255	255	255	255
Blue Mean	127.267303466797	31.7929229736328	124.046249389648	**126.954391479492**
Blue Standard Deviation	41.4810548080386	58.8056941224182	33.4094076505899	**44.2130332332022**
Blue Median	128	0	126	**129**
Blue Total Count	65536	65536	65536	65536
Saturation Min	0	0	0	0
Saturation Max	0	0	0	0
Saturation Mean	0	0	0	0
Saturation Standard Deviation	0	0	0	0
Saturation Median	0	0	0	0
Luminance Min	0	0	0	0
Luminance Max	1	1	1	1
Luminance Mean	0.499087452888489	0.124678127467632	0.486455887556076	0.497860372066498
Luminance Standard Deviation	0.162670806050301	0.230610564351082	0.131017282605171	0.173384442925453
Luminance Median	0.501960813999176	0	0.494117647409439	0.505882382392883
Y Min	0	0	0	0
Y Max	1	1	1	1
Y Mean	0.499087452888489	0.124678127467632	0.486455887556076	0.497860372066498
Y Standard Deviation	0.162670806050301	0.230610564351082	0.131017282605171	0.173384442925453
Y Median	0.501960813999176	0	0.494117647409439	0.505882382392883
Cb Min	-0.00196078419685364	-0.00196078419685364	-0.00196078419685364	-0.00196078419685364
Cb Max	-0.00196078419685364	-0.00196078419685364	-0.00196078419685364	-0.00196078419685364
Cb Mean	-0.00196078442968428	-0.00196078442968428	-0.00196078442968428	-0.00196078442968428
CbStandardDeviation	1.15958798119209E-10	1.15958798119209E-10	1.15958798119209E-10	1.15958798119209E-10
Cb Median	-0.00196078419685364	-0.00196078419685364	-0.00196078419685364	-0.00196078419685364
Cr Min	-0.00196078419685364	-0.00196078419685364	-0.00196078419685364	-0.00196078419685364
Cr Max	-0.00196078419685364	-0.00196078419685364	-0.00196078419685364	-0.00196078419685364

Cr Mean	-0.00196078442968428	-0.00196078442968428	-0.00196078442968428	-0.00196078442968428
Cr Standard Deviation	1.15958798119209E-10	1.15958798119209E-10	1.15958798119209E-10	1.15958798119209E-10
Cr Median	-0.00196078419685364	-0.00196078419685364	-0.00196078419685364	-0.00196078419685364
Red Min WB	1	2	1	2
Red Max WB	255	255	255	255
Red Mean WB	127.530007186434	127.412768299395	124.974941966825	130.115147629176
Red Standard Deviation WB	41.1184521169296	40.9325210351901	31.7566016273799	39.9023570461158
Red Median WB	128	128	126	130
Red Total Count WB	65401	16353	65049	63944
Green Min WB	1	2	1	2
Green Max WB	255	255	255	255
Green Mean WB	127.530007186434	127.412768299395	124.974941966825	130.115147629176
Green Standard Deviation WB	41.1184521169296	40.9325210351901	31.7566016273799	39.9023570461158
Green Median WB	128	128	126	130
Green Total Count WB	65401	16353	65049	63944
Blue Min WB	1	2	1	2
Blue Max WB	255	255	255	255
Blue Mean WB	127.530007186434	127.412768299395	124.974941966825	130.115147629176
Blue Standard Deviation WB	41.1184521169296	40.9325210351901	31.7566016273799	39.9023570461158
Blue Median WB	128	128	126	130
Blue Total Count WB	65401	16353	65049	63944
Saturation Min WB	0	0	0	0
Saturation Max WB	0	0	0	0
Saturation Mean WB	0	0	0	0
Saturation Standard Deviation WB	0	0	0	0
Saturation Median WB	0	0	0	0
Luminance Min WB	0.00392156885936856	0.00784313771873713	0.00392156885936856	0.00784313771873713
Luminance Max WB	1	1	1	1
Luminance Mean WB	0.500117659568787	0.499657928943634	0.49009782075882	0.510255455970764
Luminance Standard Deviation WB	0.161248832941055	0.160519689321518	0.124535694718361	0.156479835510254
Luminance Median WB	0.501960813999176	0.501960813999176	0.494117647409439	0.509803950786591
Y Min WB	0.00392156885936856	0.00784313771873713	0.00392156885936856	0.00784313771873713
Y Max WB	1	1	1	1
Y Mean WB	0.500117659568787	0.499657928943634	0.49009782075882	0.510255455970764
Y Standard Deviation WB	0.161248832941055	0.160519689321518	0.124535694718361	0.156479835510254
Y Median WB	0.501960813999176	0.501960813999176	0.494117647409439	0.509803950786591
Cb Min WB	-0.00196078419685364	-0.00196078419685364	-0.00196078419685364	-0.00196078419685364
Cb Max WB	-0.00196078419685364	-0.00196078419685364	-0.00196078419685364	-0.00196078419685364
Cb Mean WB	-0.00196078442968428	-0.00196078442968428	-0.00196078442968428	-0.00196078442968428
Cb Standard Deviation WB	1.15958798119209E-10	1.15958798119209E-10	1.15958798119209E-10	1.15958798119209E-10
Cb Median WB	-0.00196078419685364	-0.00196078419685364	-0.00196078419685364	-0.00196078419685364
Cr Min WB	-0.00196078419685364	-0.00196078419685364	-0.00196078419685364	-0.00196078419685364
Cr Max WB	-0.00196078419685364	-0.00196078419685364	-0.00196078419685364	-0.00196078419685364
Cr Mean WB	-0.00196078442968428	-0.00196078442968428	-0.00196078442968428	-0.00196078442968428
Cr Standard Deviation WB	1.15958798119209E-10	1.15958798119209E-10	1.15958798119209E-10	1.15958798119209E-10
Cr Median WB	-0.00196078419685364	-0.00196078419685364	-0.00196078419685364	-0.00196078419685364

Observations
1. Median values become '0' for subsampled image. This phenomenon has been seen for all kinds of images.
2. The reconstructed image using prediction formula is pretty much closer to the original image.
3. The reconstructed image using extended morphological filter is pretty much closer to the original image.
4. There is an increase in the contrast in the reconstructed image when compared to the original image.

Fig. 11 shows a graphical presentation of the values of mean, standard deviation and median for red, green and blue components of the original radargram slice image, its subsampled image and the prediction formula and morphological filter based reconstructed images.

127.267303466797	31.7929229736328	124.046249389648	**126.954391479492**
41.4810548080386	58.8056941224182	33.4094076505899	**44.2130332332022**
128	0	126	**129**
127.267303466797	31.7929229736328	124.046249389648	**126.954391479492**
41.4810548080386	58.8056941224182	33.4094076505899	**44.2130332332022**
128	0	126	**129**
127.267303466797	31.7929229736328	124.046249389648	**126.954391479492**
41.4810548080386	58.8056941224182	33.4094076505899	**44.2130332332022**
128	0	126	**129**

Fig. 11: Graphical presentation of the values of mean, standard deviation and median for red, green and blue components of the radargram image, its subsampled image and the prediction formula and morphological filter based reconstructed images

Fig. 12 shows the differential errors introduced by both prediction techniques in certain statistical parameter values.

Fig. 12: Differential errors caused by interpolant prediction techniques

3. Conclusions

Two methods for predicting interpolant pixel values of a subsampled image (i) interpolant prediction using neighborhood pixel value averaging and (ii) interpolant prediction using extended morphological filtering are discussed briefly in this paper with real time sample images. While both methods yield appreciable results, interpolant prediction using extended morphological filtering seems to be better than the interpolant prediction using neighborhood averaging, in the sense of prediction accuracy.

Acknowledgement

Advisory Committee Members and Co-authors

1. Dr. Manish Prateek, Dean, School of Computer Science, UPES, Dehradun, India
2. Dr. Amit Agarwal, Director, APJ Abdul Kalam, Institute of Technology, Dehradun, India
3. Dr. Michael Patrick Coyle, Chief Executive Officer, Avatar MedVision US LLC, NC, USA
4. Sathya Govindarajan, Director, Pentagram Research Centre Private Limited, Hyderabad, India
5. Prashanthi Govindarajan, Director, Pentagram Research Centre Private Limited, Hyderabad, India
6. Yashaswi Vemuganti, Consultant, Avatar MedVision US LLC, NC, USA
7. Dr. Jean Claude Perez, IBM European Research Center on Artificial Intelligence, France
8. Dr. Hindupur Rajasimha, Chief Engineer, Indian Space Research Organization and IDBI (Retd.)

References

[1] Jean Serra; Cube, cube-octahedron or rhomb-dodecahedron as bases for 3-D shape descriptions, Advances in visual form analysis, World Scientific 1997, 502-519.

[2] Wuthrich, C.A. and Stucki, P.; An algorithm comparison between square- and hexagonal based grids; Graphical Models and Image Processing, 53(4), 324–339,1991.

[3] Reinhard Klette and Azriel Rosenfeld; Digital Geometry: Geometric methods for picture analysis; Elsevier, 2004.

[4] B. Nagy; Geometry of Neighborhood sequences in hexagonal grid; Discrete Geometry of computer imagery; LNCS-4245, Springer.

[5] Tristan Roussillon, Laure Tougne, and Isabelle Sivignon; What Does Digital Straightness tell about Digital Convexity?;

[6] Edward Angel, "Interactive Computer Graphics- a top down approach with OpenGL", Second Edition, Addison Wesley, 2000.

[7] S.W. Zucker, R.A. Hummel, "A Three-Dimensional Edge Operator", IEEE Trans. On PAMI, Vol. 3, May 1981.

[8] Jürgen, H., Manner, R., Knittel, G., and Strasser, W. (1995). Three Architectures for Volume Rendering. International Journal of the Eurographics Association, 14, 111-122

[9] Dachille, F. (1997). Volume Visualization Algorithms and Architectures. Research Proficiency Examination, SUNY at Stony Brook

[10] Günther, T., Poliwoda, C., Reinhart, C., Hesser, J., and Manner, J. (1994). VIRIM: A Massively Parallel Processor for Real-Time Volume Visualization in Medicine. Proceedings of the 9th Eurographics Hardware Workshop, 103-108

[11] Boer, M.De, Gröpl, A., Hesser, J., and Manner, R. (1996). Latency-and Hazard-free Volume Memory Architecture for Direct Volume Rendering. Eurographics Workshop on Graphics Hardware, 109-119

[12] Swan, J.E. (1997). Object Order Rendering of Discrete Objects. PhD. Thesis, Department of Computer and Information Science, The Ohio State University

[13] Yagel, R. (1996). Classification and Survey of Algorithms for Volume Viewing. SIGGRAPH tutorial notes (course 34)

[14] Law, A. (1996). Exploiting Coherency in Parallel Algorithms for Volume Rendering. PhD. Thesis, Department of Computer and Information Science, The Ohio State University

[15] Ray, H., Pfister, H., Silver, D., and Cook, T.A. (1999). Ray Casting Architectures for Volume Visualization.

IEEE Transactions on Visualization and Computer Graphics, 5(3), 210-233

[16] Yagel, R. (1996). Towards Real Time Volume Rendering. Proceedings of GRAPHICON' 96, 230-241

[17] Kaufman, A.E. (1994). Voxels as a Computational Representation of Geometry. in The Computational Representation of Geometry SIGGRAPH '94 Course Notes

[18] Lacroute, P., and Levoy, M. (1994). Fast Volume Rendering Using a Shear-Warp Factorization of the Viewing Transform. Computer Graphics Proceedings Annual Conference Series ACM SIGGRAPH, 451-458.

[19] Sutherland, I.E., Sproull, R.F., and Schumaker, R.A. (1974) A Characterization of Ten Hidden Surface Algorithms. ACM Computing Surveys, 6(1), 1-55

[20] Roberts, J.C. (1993). An Overview of Rendering from Volume Data including Surface and Volume Rendering. Technical Report 13-93*, University of Kent, Computing Laboratory, Canterbury, UK.

[21] Frieder, G., Gordon, D., and Reynolds, R.A. (1985). Back-to-Front Display of Voxel-Based Objects. IEEE Computer Graphics and Applications, 5(1), 52-60

[22] Westover, A.L. (1991). Splatting: A Parallel Feed-Forward Volume Rendering Algorithm. Ph.D. Dissertation, Department of Computer Science, The University of North Carolina at Chapel Hill

[23] Zwicker, M., Pfister., H., Baar, J.B. and Gross M. (2001). Surface Splatting. In Computer Graphics SIGGRAPH 2001 Proceedings, 371-378

[24] Nulkar, M., and Mueller, K. (2001). Splatting With Shadows. International Workshop on Volume Graphics 2001,35-50

[25] J. Krüger and R. Westermann, Acceleration Techniques for GPU-based Volume Rendering, Proceedings of the 14th IEEE Visualization 2003 (VIS'03), 38-43.

[26] Markus Hadwiger, Joe M. Kniss, Christ of Rezk-salama, Daniel Weiskopf, and Klaus Engel. Real time Volume Graphics. A. K. Peters, Ltd., USA, 2006.

[27] Goodman, D., Nishimura, Y., Hongo, H and Noriaki N., 2006. Correcting for topography and the tilt of the GPR antenna, Archaeological Prospection, 13: 157-161.

[28] Goodman, D., Y. Nishimura, and J. D. Rogers, 1995. GPR time slices in archaeological prospection: *Archaeological Prospection*, 2:85-89.

[29] Goodman, D., 1994. Ground-penetrating radar simulation in engineering and archaeology: *GEOPHYSICS,* 59:224-232.